RSC Advances

PAPER

View Article Online
View Journal | View Issue

Cite this: *RSC Adv.*, 2023, **13**, 16567

A CMC-*g*-poly(AA-*co*-AMPS)/Fe_3O_4 hydrogel nanocomposite as a novel biopolymer-based catalyst in the synthesis of 1,4-dihydropyridines†

Elmira Hemmati, Somayeh Soleimani-Amiri * and Mehran Kurdtabar *

Received 1st March 2023
Accepted 15th May 2023

DOI: 10.1039/d3ra01389h

rsc.li/rsc-advances

A CMC-*g*-poly(AA-*co*-AMPS)/Fe_3O_4 hydrogel nanocomposite was successfully designed and prepared *via* graft copolymerization of AA and AMPS on CMC followed by the cross-linking addition of $FeCl_3$/$FeCl_2$. The synthesized hydrogel nanocomposite was characterized by Fourier-transform infrared (FT-IR) spectroscopy, scanning electron microscopy (SEM), transmission electron microscopy (TEM), energy-dispersive X-ray (EDX) spectroscopy, elemental mapping, thermogravimetric analysis/differential thermal analysis (TGA/DTA), and vibrating sample magnetometry (VSM). The CMC-*g*-poly(AA-*co*-AMPS)/Fe_3O_4 hydrogel nanocomposite was employed as a biocompatible catalyst for the green synthesis of 1,4-dihydropyridine (1,4-DHP) derivatives under thermal and ultrasound-assisted reaction conditions. High efficiency, low catalyst loadings, short reaction time, frequent catalyst recovery, environmental compatibility and mild conditions were found in both methods.

Introduction

Green chemistry is considered to increase the use of green and non-toxic materials. Applying catalytic methods in organic synthesis has become a very deep research field. The increasing need for reaction systems with catalytic green aspects and benign echo progress and advancement of eco-benign, cost-effective, high-atom-economy, and high-yield processes is highly desirable.[1–3]

The study, synthesis, and application of hybrid materials have been one of the active research areas in recent years due to their superior properties and high application potential.[4] Hydrogel-based hybrid materials are generally easy to design and manufacture.[5,6] Supramolecular hydrogels could be used as matrices for placing nanoparticles in nanocomposite gel hybrid materials.[7–9] Metal, non-metal or polymer nanoparticles (NPs) are widely used in the hydrogel matrix to formulate nanocomposites. The nanoparticles can yield nanocomposites with special properties such as magnetic, antibacterial, and catalytic activities.[10–15] However, rigid hydrogel matrices can reduce nanomaterial size and chemical and physical stability, facilitating handling, recovery, and reuse. Nanoparticle-gel hybrid materials have widespread applications including biosensors, chiral catalysts, and nonlinear optics. Hydrogel matrices could also perfectly reduce aggregation and improve biocompatibility, especially for magnetic nanoparticles. Various polysaccharides including polyvinyl alcohol (PVA), chitosan, and carboxymethyl cellulose (CMC) have been investigated.[16,17]

Multi-component reactions (MCRs) are known as an influential and potent tool for the design and synthesis of a wide range of organic compounds, especially biologically active heterocycles.[3,18–21] These are evaluated as valuable and efficient methods due to the time-saving, atom-economy, and environmentally friendly nature.[22–26] The Hantzsch reaction has been identified as one of the most widely used and effective multi-component reactions for the synthesis of 1,4-dihydropyridine (1,4-DHP) derivatives. 1,4-DHP derivatives, as important nitrogen-containing heterocyclic compounds, displayed valuable pharmaceutical and biological activities. These are applied as anti-tumor, anti-hypertensive, anti-platelet aggregation, bronchodilator, neuroprotective drugs and so on. Moreover, calcium channel blockers such as felodipine, nifedipine, nimodipine, nicardipine, and amlodipine owe their medicinal properties to the 4-aryl-1,4-dihydropyridine moiety.[27,28] Therefore, the influential role of 1,4-DHP derivatives in the design of new drugs is intelligible. Consequently, their synthesis is one of the recent research challenges in chemistry and pharmaceuticals.

As an alternative energy source, ultrasound waves accelerate chemical reactions *via* the formation and collapse of transient cavitation bubbles.[29,30] Ultrasonic waves create high-energy hot spots, which reactant molecules absorb. Accordingly, sufficient energy is provided to overcome the reaction activation barrier, which accelerates the reaction. Thus, ultrasound-promoted reactions are expected to indicate advantages such as high chemical reactivity, high selectivity, a clean reaction process, excellent product yields, and short reaction time.[31–34]

Department of Chemistry, Karaj Branch, Islamic Azad University, Karaj, Iran. E-mail: s.soleimani@kiau.ac.ir; m.kurdtabar@kiau.ac.ir

† Electronic supplementary information (ESI) available. See DOI: https://doi.org/10.1039/d3ra01389h

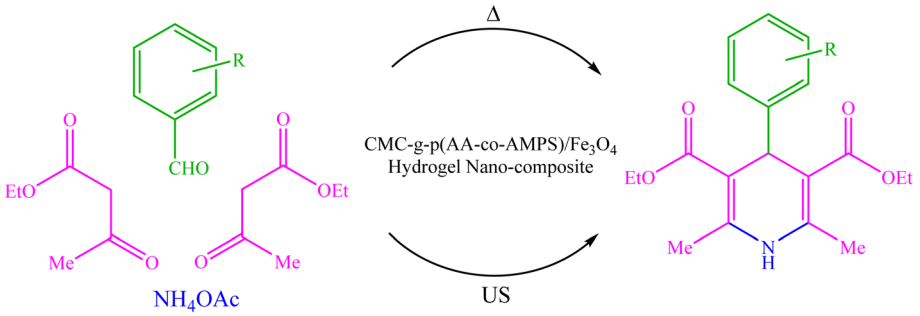

Scheme 1 Hantzsch synthesis of 1,4-DHP derivatives using CMC-*g*-poly(AA-*co*-AMPS)/Fe_3O_4 hydrogel nanocomposite under both thermal and ultrasonic conditions.

Due to the recent challenges, new protocols for efficiently synthesizing 1,4-DHP derivatives under environmentally safe conditions are still demanded. In continuation of our previous works on the synthesis and application of nanocatalysts in heterocyclic synthesis,[35–43] herein we wish to report the design, synthesis, and use of biopolymer-based CMC-*g*-poly(AA-*co*-AMPS)/Fe_3O_4 hydrogel nanocomposites in the Hantzsch

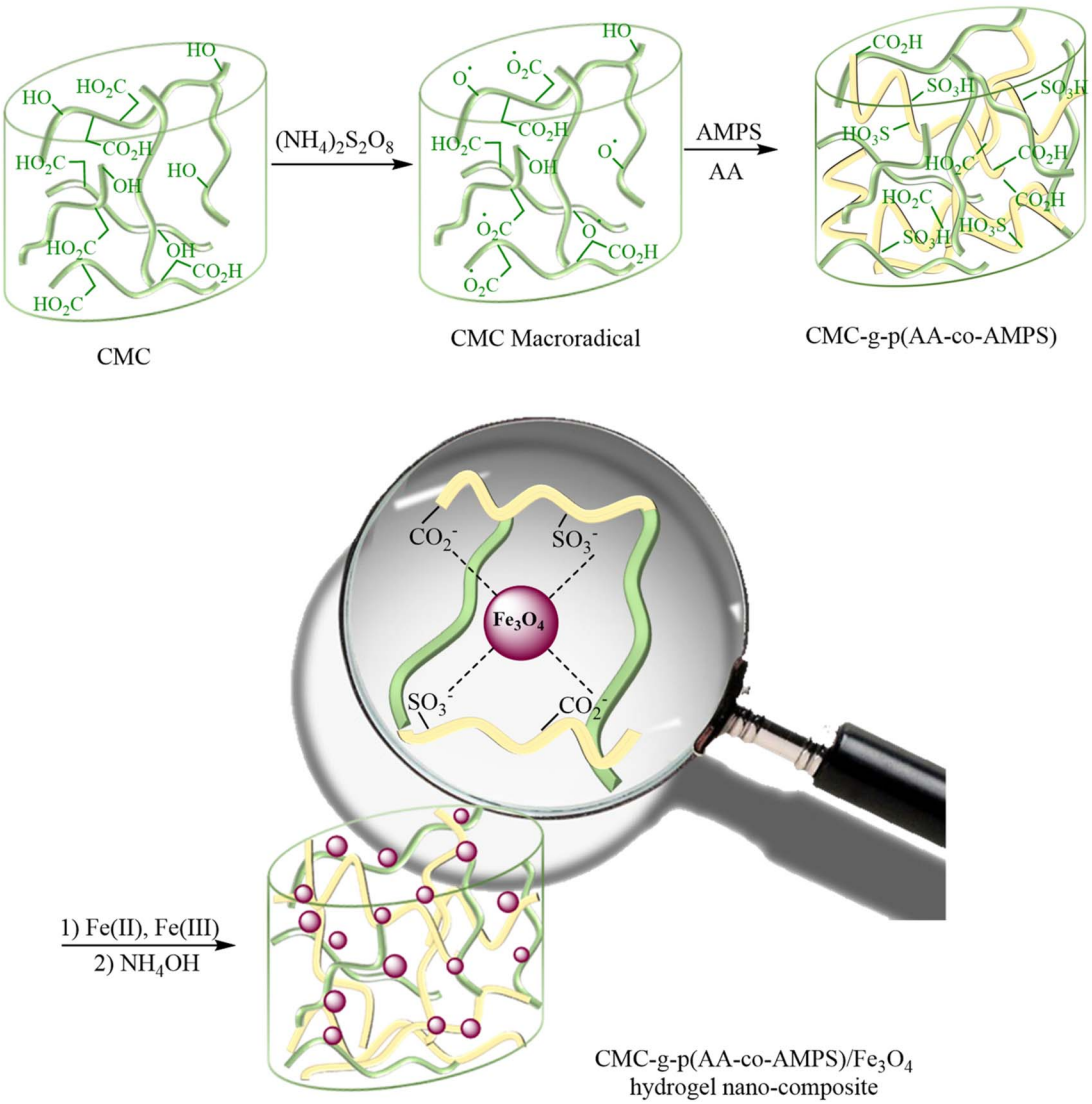

Scheme 2 Synthesis of the CMC-*g*-poly(AA-*co*-AMPS)/Fe_3O_4 hydrogel nanocomposite.

synthesis of 1,4-DHP derivatives under both thermal and ultrasound-assisted conditions (Scheme 1).

Result and discussion

The CMC-*g*-poly(AA-*co*-AMPS)/Fe_3O_4 hydrogel nanocomposite was synthesized in the following two steps: (1) graft copolymerization of acrylic acid (AA) and 2-acrylamido-2-methylpropane sulfonic acid (AMPS) onto carboxymethyl cellulose (CMC) in the presence of ammonium persulfate (APS); (2) $FeCl_3$/$FeCl_2$ augmenting as cross-linking agents (Scheme 2). The graft copolymerization reaction was initiated *via* the generated sulfate anion radicals due to the thermal decomposition of APS. Sulfate anion radicals developed alkoxy radicals of CMC, copolymerized with AA and AMPS monomers. A three-dimensional network structure of CMC-*g*-poly(AA-*co*-AMPS)/Fe_3O_4 hydrogel nanocomposites was produced *via* the interaction of $-CO_2^-$ and $-SO_3^-$ chelating moieties from the copolymer and added $Fe^{(2+)}$ and $Fe^{(3+)}$ ions under the basic condition.[16,17,44–47]

The FT-IR spectra of bare CMC and CMC-*g*-poly(AA-*co*-AMPS)/Fe_3O_4 hydrogel nanocomposites were studied in 4000–400 cm^{-1} (Fig. 1). The FT-IR spectrum of bare CMC indicated that the peaks observed at 1427 and 1622 cm^{-1} were assigned to the symmetric and asymmetric stretching vibrations of CO_2^- groups (Fig. 1a). The explicit broad peak at 3434 cm^{-1} was attributed to the O–H stretching vibrations.[16] Additional signals were detected for the CMC-*g*-poly(AA-*co*-AMPS)/Fe_3O_4 hydrogel nanocomposite (Fig. 1b). The identified peaks at 1733, 1179, and 1035 cm^{-1} were assigned to C=O in AA, and the asymmetric and symmetric stretching vibrations of S=O in AMPS, respectively. The observed shifts of C=O and S=O groups could be attributed to the interaction of O atoms of carboxylic and sulfonic acid due to charge transfer interactions with Fe_3O_4 nanoparticles.[48] The Fe_3O_4 nanoparticles were stabilized inside the CMC hydrogel network *via* the interactions.

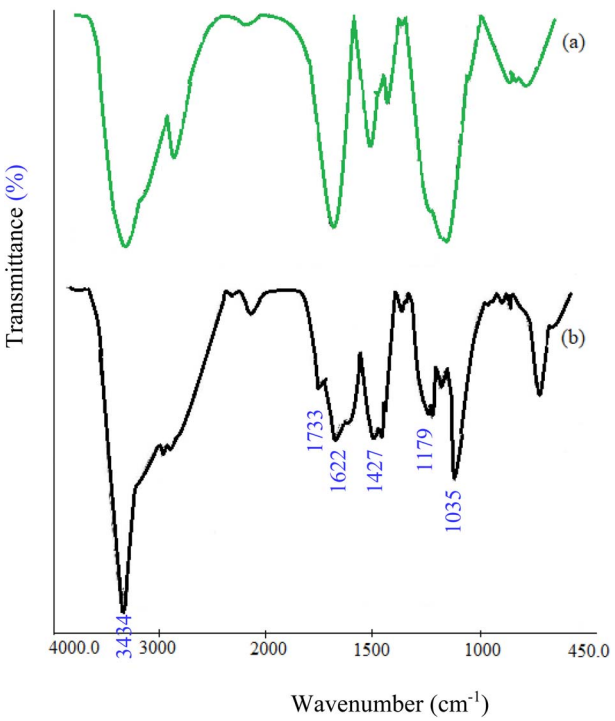

Fig. 1 Comparative FT-IR spectra of (a) bare CMC and (b) CMC-*g*-poly(AA-*co*-AMPS)/Fe_3O_4 hydrogel nanocomposite.

Scanning electron microscopy (SEM) and transmission electron microscopy (TEM) were considered as visual evidence of the shape, size and distribution of Fe_3O_4 nanoparticles on the surface and embedded in the CMC-*g*-poly(AA-*co*-AMPS) hydrogel matrix, respectively (Fig. 2). The images displayed no aggregation for Fe_3O_4 nanoparticles, indicating that the nanoparticles were uniformly embedded on the surface and within the CMC-*g*-poly(AA-*co*-AMPS) hydrogel matrix. The nanoparticles appeared nearly spherical, with an average diameter of about 18 nm. The identical dispersion of nanoparticles with homogeneous shapes and sizes among the hydrogel network is due to the network's uniform mesh size and distribution of functional groups. The small size favorably affects the number, surface area, and specific surface area of nanoparticles, while the aggregated/agglomerated nanoparticles significantly weaken the positive attributes of nanoparticles in nanocomposites. This occurrence affects the characteristics of nanoparticles and interface, which finally change the behavior of nanocomposites.[49] Accordingly, a strong chemical interaction was found between the carboxylate and sulfonate ions of the CMC-*g*-poly(AA-*co*-AMPS) hydrogel matrix and Fe_3O_4 nanoparticles due to the small particle size.[50]

Fe_3O_4 nanoparticles embedded in the CMC-*g*-poly(AA-*co*-AMPS) polymer were confirmed by energy-dispersive X-ray (EDX) analysis (Fig. 3a). The EDX spectrum of the CMC-*g*-poly(AA-*co*-AMPS)/Fe_3O_4 hydrogel nanocomposite identified the presence of carbon (50.2%), sulfur (29.5%), and oxygen atoms in the hydrogel matrix, as well as iron (6.8%) and oxygen atoms of nanoparticles. Additionally, the dispensation pattern of structural elements in the CMC-*g*-poly(AA-*co*-AMPS)/Fe_3O_4 hydrogel nanocomposite was well detected using elemental mapping, which confirmed the uniform Fe_3O_4 distribution on the CMC-*g*-poly(AA-*co*-AMPS)/Fe_3O_4 hydrogel nanocomposite surface (Fig. 3b).

Thermogravimetric analysis (TGA) and differential thermal analysis (DTA) of the CMC-*g*-poly(AA-*co*-AMPS)/Fe_3O_4 hydrogel nanocomposite were performed at 0–800 °C in an N_2 atmosphere (Fig. 4). The first weight loss was observed at 150 °C, related to the removal of hydrogel moisture. The maximum degradation rate occurred between 250 and 350 °C, related to polymer degradation by intramolecular reactions such as esterification, anhydration, and the like between functional groups that exist in the polymer backbone. The remaining polymer components were completely broken down at 350–800 °C. Finally, 14.75% of the hydrogel remained at 800 °C, which can be attributed to the nanoparticles in the hydrogel.

The recycled hydrogel nanocomposite implied amplified magnetic properties compared to the fresh sample by increasing the magnetic saturation value (M_s) to 1.55 emu g^{-1}, with nonzero remanent magnetization (M_r) and coercivity (C_e), indicating ferromagnetism behavior (Fig. 5b).[51,52] The enhanced magnetic property, nonzero remanent magnetization, and

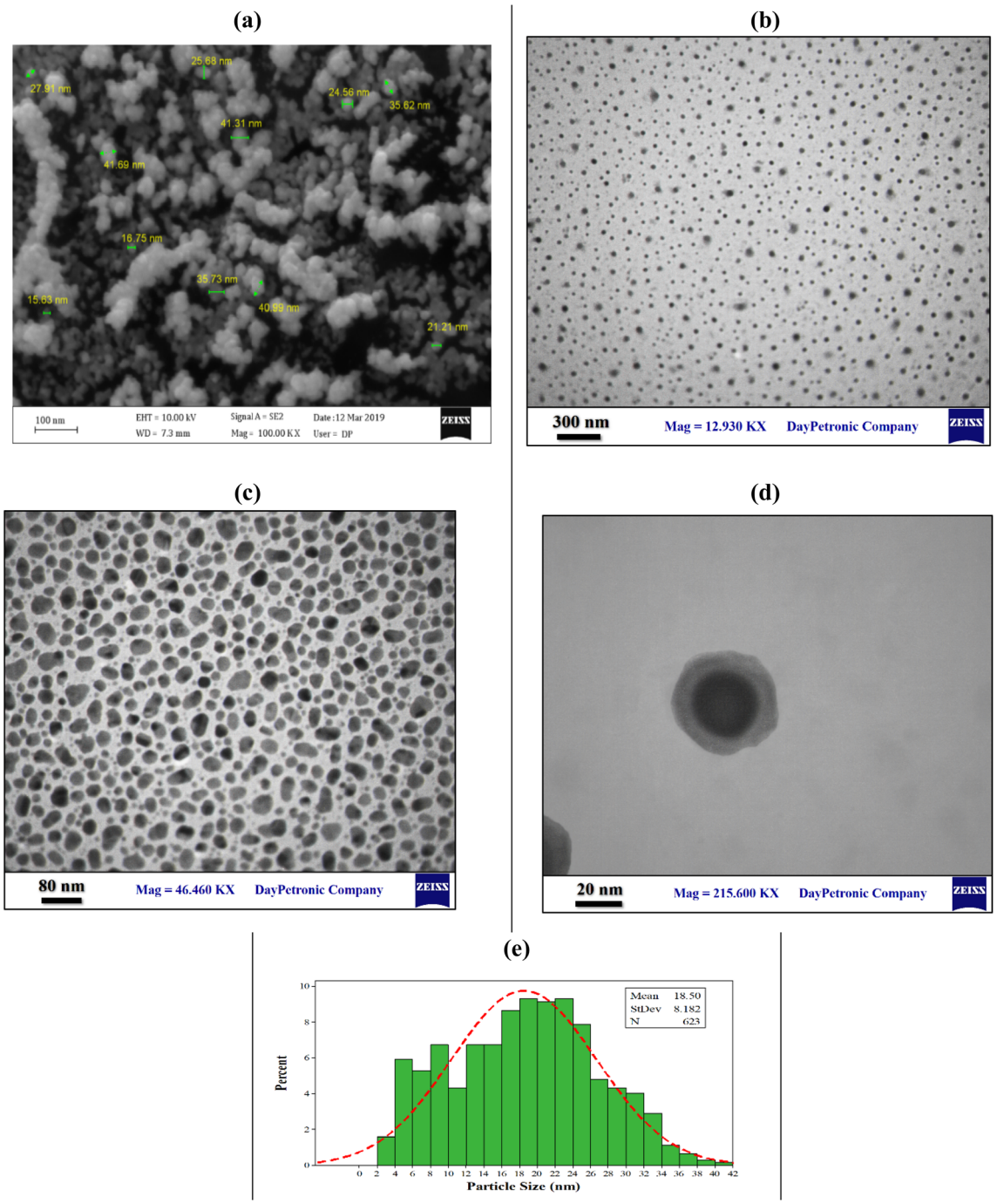

Fig. 2 SEM image (a), TEM images (b–d), and size distribution (e) of the CMC-*g*-poly(AA-*co*-AMPS)/Fe_3O_4 hydrogel nanocomposite.

coercivity for the recycled hydrogel nanocomposite were probably due to the partial degradation of the hydrogel and the release of Fe_3O_4 nanoparticles.[52,53]

The produced CMC-*g*-poly(AA-*co*-AMPS)/Fe_3O_4 hydrogel nanocomposite was evaluated as a catalyst for the Hantzsch synthesis of 1,4-dihydropyridine (1,4-DHP) under thermal and ultrasound-assisted conditions (Scheme 1). The effects of catalyst loading, solvent, and temperature were investigated to optimize the model reaction parameters of diethyl-2,6-dimethyl-4-phenyl-1,4-dihydropyridine-3,5-dicarboxylate synthesis (Table 1). While low yields of products were detected in H_2O, EtOH, $PhCH_3$, CH_2Cl_2, and CH_3CN solvents, solvent-free conditions resulted in good efficiency in 20 min (Table 1, entries 1–6). Then, a series of equivalent reactions with different catalyst loadings were used to investigate the role of CMC-*g*-poly(AA-*co*-AMPS)/Fe_3O_4 hydrogel nanocomposites in the reaction rate and efficiency (Table 1, entries 6–10). A gradual increase in catalyst loading (0–30 wt%) was scrutinized. Only a small amount of product was acquired without the hydrogel nanocomposite, while the maximum efficiency was found due

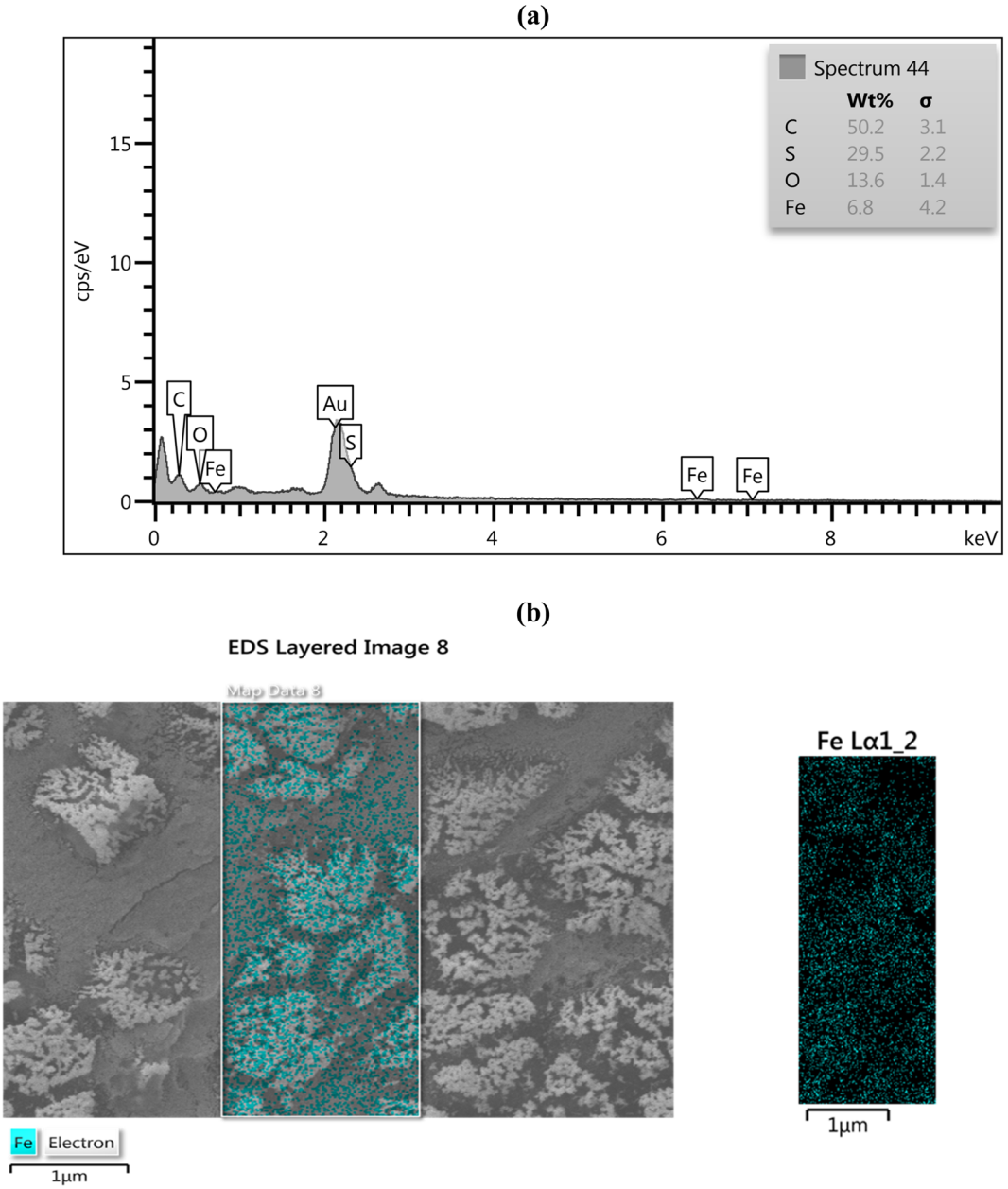

Fig. 3 EDX analysis (a) and (b) elemental mapping of the CMC-*g*-poly(AA-*co*-AMPS)/Fe_3O_4 hydrogel nanocomposite.

to 10 wt% catalyst loading. The reaction yield was estimated to be almost constant with a further increase in the amount of catalyst (Table 1, entries 6–10). Next, the model reaction was evaluated with similar conditions and catalyst loadings at different temperatures (Table 1, entries 11–13). Notably, the most appropriate outcome was obtained at 80 °C. Finally, the best time to perform the reaction was estimated to be about 20 min (Table 1, entries 14 and 15).

Additionally, the model reaction was explored under ultrasound conditions (Table 1, entries 16–24). Ultrasonic waves improved the reaction, so that the reaction was carried out at 40 °C with a higher efficiency than that under thermal conditions (Table 1, entry 21).

Several aryl/heteroaryl aldehydes were carried out in the Hantzsch synthesis of 1,4-DHP using CMC-*g*-poly(AA-*co*-AMPS)/Fe_3O_4 hydrogel nanocomposites (10 wt%) under thermal and ultrasonic conditions to assay the scope of the current protocol (Table 2). The synthesis of 1,4-DHP derivatives was performed under optimal conditions with various aryl aldehydes containing electron-withdrawing and electron-donating groups as well as halogens with high efficiency and at the right time. Aryl aldehydes containing electron-donor groups decreased the reaction rate, while electron-acceptor groups and halogens indicated a greater tendency to carry out the Hantzsch reaction. Moreover, high yields of products were found for heteroaryl aldehydes (Table 2, entries 17–20).[28,54–60]

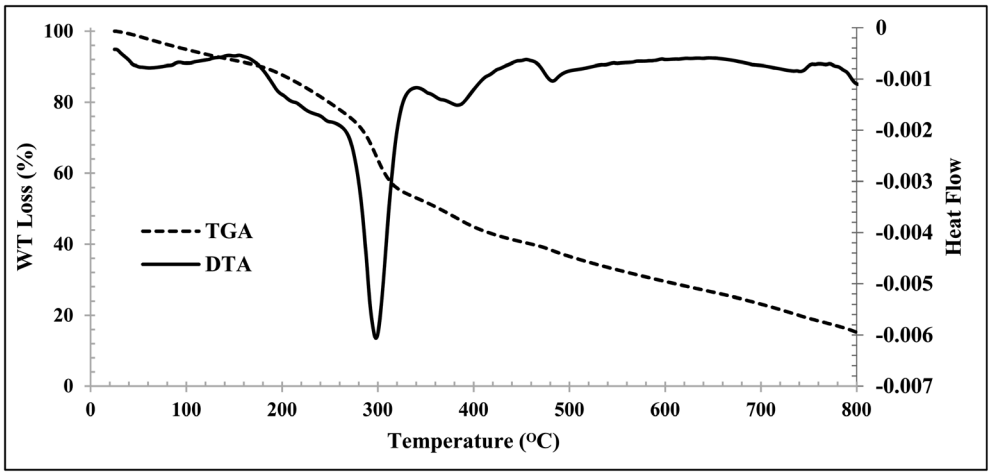

Fig. 4 TGA (dash line) and DTG (solid line) analysis of the CMC-*g*-poly(AA-*co*-AMPS)/Fe_3O_4 hydrogel nanocomposite.

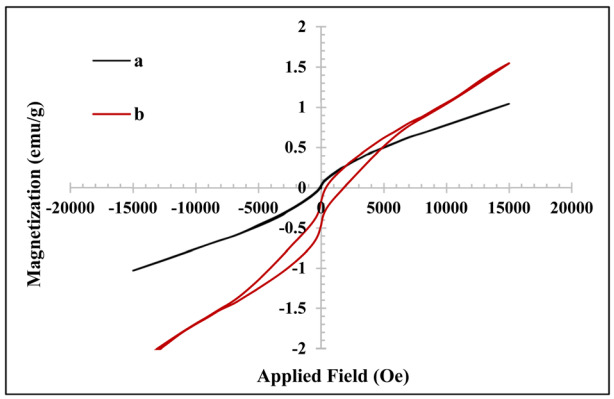

Fig. 5 VSM diagram of (a) a fresh CMC-*g*-poly(AA-*co*-AMPS)/Fe_3O_4 hydrogel nanocomposite and (b) recycled CMC-*g*-poly(AA-*co*-AMPS)/Fe_3O_4 hydrogel nanocomposite after six times.

Recently, the application of nanocatalysts in organic synthesis has been considered. Table 3 presents the comparative performance of the CMC-*g*-poly(AA-*co*-AMPS)/Fe_3O_4 hydrogel nanocomposite and other nanocatalysts previously used in the Hantzsch synthesis of 1,4-dihydropyridine. The results introduced the CMC-*g*-poly(AA-*co*-AMPS)/Fe_3O_4 hydrogel nanocomposite as one of the most efficient nanocatalysts in the Hantzsch synthesis of 1,4-dihydropyridine under conventional and ultrasound-assisted conditions (Table 3, entries 10 and 11).[28,55,58,61–66]

Catalyst recycling is one of the most important advantages that make catalysts important for commercial applications. Therefore, the recyclability of the CMC-*g*-poly(AA-*co*-AMPS)/Fe_3O_4 hydrogel nanocomposite in the Hantzsch reaction under optimized conditions was investigated (Fig. 6). The hydrogel nanocomposite can be applied at least six times without significantly decreasing the catalytic activity in this reaction.

There was a plausible mechanism proposed for the synthesis of 1,4-dihydropyridine (1,4-DHP) using the CMC-*g*-poly(AA-*co*-AMPS)/Fe_3O_4 hydrogel nanocomposite (Scheme 3).[27] Ethyl acetoacetate (EAA) reacted with the activated aldehyde *via* Knoevenagel condensation to form intermediate **A**. Intermediate **B** was obtained from ammonium acetate and the second equivalent of EAA in an acidic medium. The CMC-*g*-poly(AA-*co*-AMPS)/Fe_3O_4 hydrogel nanocomposite catalyzed Michael's addition and reactions of intermediates **A** and **B**. Finally, cyclocondensation of intermediate **C** was performed to obtain the product.

Experimental

Materials and equipment

All materials and reagents were purchased from reputable commercial companies including Merck, Sigma-Aldrich, and Alfa-Aesar and then used without further purification. TLC was performed to monitor the purity of the synthesized compounds. IA 9200 Electrothermal apparatus was used to evaluate the melting points without any correction. FT-IR spectra were recorded using a PerkinElmer spectrometer with KBr disks at 400–4000 cm^{-1}. A Model LBKFB from Desert Precision Magnet Company was used for vibrating sample magnetometry (VSM) at room temperature to study the magnetic properties. The elements were determined using a Numerix DXP-X10P energy-dispersive X-ray spectrometer (EDX). Scanning electron microscopic (SEM) images were obtained using a SIGMA VP-500-Zeiss. Transmission electron microscopy (TEM) was carried out using a Zeiss-EM10C microscope operating at an accelerating voltage of 100 kV. Thermogravimetric analysis (TGA) was performed at 15–800 °C in a nitrogen atmosphere using a PerkinElmer instrument of Pyris 1PT-1600. A WUC-A03H from Daihan Scientific Company was employed for ultrasonic waves. Bruker Avance DRX-300 and DRX-75 were applied for recording ^1H and ^{13}C nuclear magnetic resonance (NMR) spectra, respectively.

Synthesis of CMC-*g*-poly(AA-*co*-AMPS)/Fe_3O_4 hydrogel nanocomposite

Sodium-carboxymethyl-cellulose (CMC) (1.0 g) was dissolved in water, and the solution was transferred to a three-necked

Table 1 The effect of catalyst loading, solvent, and temperature in the Hantzsch synthesis of diethyl-2,6-dimethyl-4-phenyl-1,4-dihydropyridine-3,5-dicarboxylate using the CMC-*g*-poly(AA-*co*-AMPS)/Fe_3O_4 hydrogel nanocomposite[a,b]

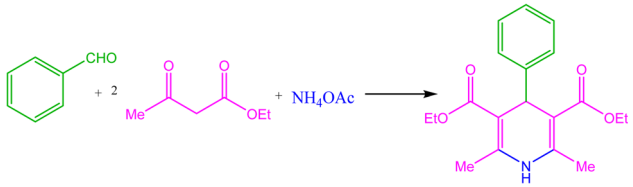

Entry	Catalyst	Catalyst loading (wt%)	Solvent	Temperature (°C)	Time (min)	Yield[c] (%)
1	CMC-*g*-poly(AA-*co*-AMPS)/Fe_3O_4[a]	10	H_2O	Reflux	20	24
2	CMC-*g*-poly(AA-*co*-AMPS)/Fe_3O_4[a]	10	EtOH	Reflux	20	82
3	CMC-*g*-poly(AA-*co*-AMPS)/Fe_3O_4[a]	10	$PhCH_3$	Reflux	20	70
4	CMC-*g*-poly(AA-*co*-AMPS)/Fe_3O_4[a]	10	CH_2Cl_2	Reflux	20	60
5	CMC-*g*-poly(AA-*co*-AMPS)/Fe_3O_4[a]	10	CH_3CN	Reflux	20	75
6	**CMC-*g*-poly(AA-*co*-AMPS)/Fe_3O_4[a]**	**10**	**—**	**80**	**20**	**87**
7	CMC-*g*-poly(AA-*co*-AMPS)/Fe_3O_4[a]	—	—	80	40	12
8	CMC-*g*-poly(AA-*co*-AMPS)/Fe_3O_4[a]	5	—	80	30	69
9	CMC-*g*-poly(AA-*co*-AMPS)/Fe_3O_4[a]	20	—	80	20	81
10	CMC-*g*-poly(AA-*co*-AMPS)/Fe_3O_4[a]	30	—	80	20	80
11	CMC-*g*-poly(AA-*co*-AMPS)/Fe_3O_4[a]	10	—	60	40	71
12	CMC-*g*-poly(AA-*co*-AMPS)/Fe_3O_4[a]	10	—	90	20	87
13	CMC-*g*-poly(AA-*co*-AMPS)/Fe_3O_4[a]	10	—	100	20	87
14	CMC-*g*-poly(AA-*co*-AMPS)/Fe_3O_4[a]	10	—	80	10	79
15	CMC-*g*-poly(AA-*co*-AMPS)/Fe_3O_4[a]	10	—	80	40	87
16	CMC-*g*-poly(AA-*co*-AMPS)/Fe_3O_4[b]	10	H_2O	Reflux	15	31
17	CMC-*g*-poly(AA-*co*-AMPS)/Fe_3O_4[b]	10	EtOH	Reflux	15	86
18	CMC-*g*-poly(AA-*co*-AMPS)/Fe_3O_4[b]	10	$PhCH_3$	Reflux	15	72
19	CMC-*g*-poly(AA-*co*-AMPS)/Fe_3O_4[b]	10	CH_2Cl_2	Reflux	15	63
20	CMC-*g*-poly(AA-*co*-AMPS)/Fe_3O_4[b]	10	CH_3CN	Reflux	15	79
21	**CMC-*g*-poly(AA-*co*-AMPS)/Fe_3O_4[b]**	**10**	**—**	**40**	**10**	**90**
22	CMC-*g*-poly(AA-*co*-AMPS)/Fe_3O_4[b]	—	—	40	20	18
23	CMC-*g*-poly(AA-*co*-AMPS)/Fe_3O_4[b]	5	—	40	20	74
24	CMC-*g*-poly(AA-*co*-AMPS)/Fe_3O_4[b]	20	—	40	15	89

[a] Reaction conditions: benzaldehyde (1 mmol), ethyl acetoacetate (2 mmol), and ammonium acetate (1.5 mmol) under thermal conditions. [b] Reaction conditions: benzaldehyde (1 mmol), ethyl acetoacetate (2 mmol), and ammonium acetate (1.5 mmol) under ultrasound-assisted conditions. [c] Isolated yields.

reactor equipped with a mechanical stirrer and set in a warm water bath at 80–85 °C. Then, 2-acrylamido-2-methylpropane sulfonic acid (AMPS) (2.0 g), ammonium persulfate (APS) (0.08 g), and acrylic acid (AA) (2.0 g) were added to the reaction mixture and allowed to polymerize for 60 min. Followed by cooling, a solution of $FeCl_3 \cdot 6H_2O/FeCl_2 \cdot 4H_2O$ (1/4) was poured dropwise into the reaction mixture. After one hour of stirring, an ammonia solution (20 mL) was added to form Fe_3O_4 nanoparticles within the polymer matrix under continuous stirring for half an hour at room temperature.

Finally, the produced CMC-*g*-poly(AA-*co*-AMPS)/Fe_3O_4 hydrogel nanocomposite was dehydrated with ethanol and then dried at 50 °C overnight.

General experimental procedure for Hantzsch synthesis using CMC-*g*-poly(AA-*co*-AMPS)/Fe_3O_4 hydrogel nanocomposites

A mixture of aryl aldehyde (1 mmol), ammonium acetate (1.5 mmol), ethyl acetoacetate (2 mmol), and CMC-*g*-poly(AA-*co*-AMPS)/Fe_3O_4 hydrogel nanocomposite (10 wt%) was added in a round-bottomed flask at 80 °C. Moreover, the reaction mixture was once again subjected to ultrasonic irradiation at 40 °C for a suitable time. The reaction progression was monitored by thin-layer chromatography (TLC). After the reaction, ethanol was applied to obtain the product. The hydrogel nanocomposite was filtered, washed, dried, and prepared for the next use. The products were purified by recrystallization with ethanol/water.

Spectral data of 1,4-dihydropyridine (1,4-DHP)

Diethyl 2,6-dimethyl-4-phenyl-1,4-dihydropyridine-3,5-dicarboxylate (4a). Mp: 158–160 °C (155–160 °C[28]); ^{1}H NMR (300 MHz, DMSO-d_6) δ (ppm): 1.11 (t, 6H, $2CH_3$), 2.25 (s, 6H, $2CH_3$), 3.96 (m, 4H, $2CH_2$), 4.85 (s, 1H, CH), 7.07–7.21 (m, 4H, Ph), 8.79 (s, 1H, NH); ^{13}C NMR (75 MHz, DMSO-d_6) δ (ppm): 14.14, 18.20, 58.95, 101.83, 125.83, 127.33, 127.81, 145.31, 148.15, 166.92.

Diethyl 2,6-dimethyl-4-(3-nitrophenyl)-1,4-dihydropyridine-3,5-dicarboxylate (4b). Mp: 164–166 °C (162 °C[28]); ^{1}H NMR (300 MHz, DMSO-d_6) δ (ppm): 1.10 (t, 6H, $2CH_3$), 2.27 (s, 6H,

Table 2 The Hantzsch synthesis of 1,4-DHPs using the CMC-*g*-poly(AA-*co*-AMPS)/Fe_3O_4 hydrogel nanocomposite

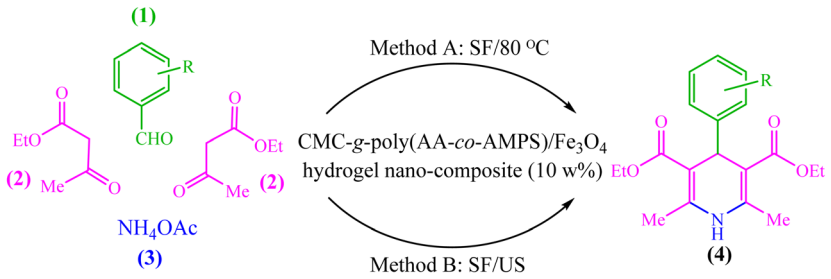

Entry	Aldehyde	Product	Method A[a] Time (min)	Method A[a] Yield[c] (%)	Method B[b] Time (min)	Method B[b] Yield[c] (%)	Mp (°C) (lit.)
1	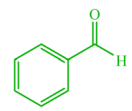	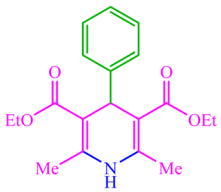 **4a**	20	87	10	90	158–160 (155–160) (28)
2	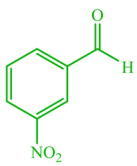	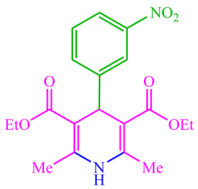 **4b**	10	90	10	93	164–166 (162) (28)
3	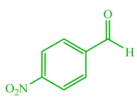	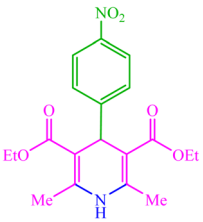 **4c**	10	90	10	95	129–133 (127–132) (28)
4	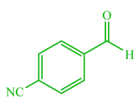	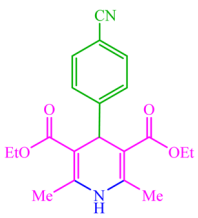 **4d**	—	—	10	80	162–166 (166–167) (54)
5	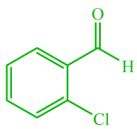	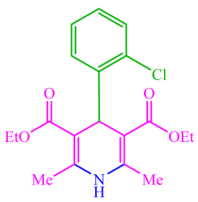 **4e**	10	80	—	—	214 (216–217) (55)

Table 2 (*Contd.*)

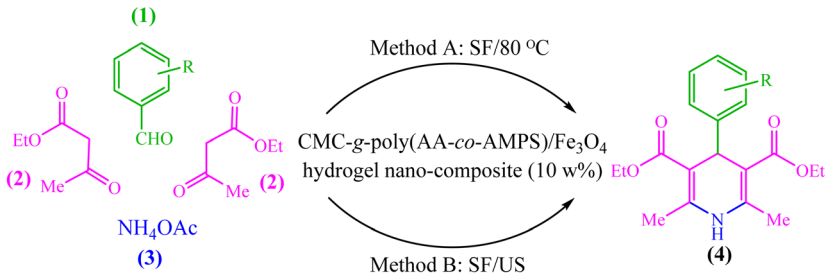

Entry	Aldehyde	Product	Method A[a] Time (min)	Method A[a] Yield[c] (%)	Method B[b] Time (min)	Method B[b] Yield[c] (%)	Mp (°C) (lit.)
6	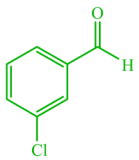	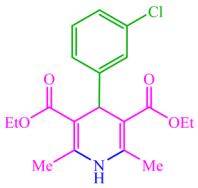 **4f**	10	85	10	90	138–140 (140) (28)
7	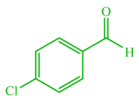	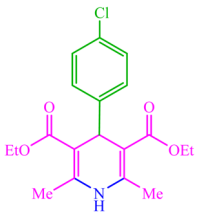 **4g**	10	87	10	98	150–154 (150–152) (56)
8	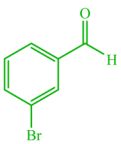	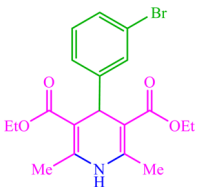 **4h**	10	77	10	85	231–235 (230) (28)
9	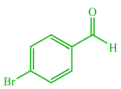	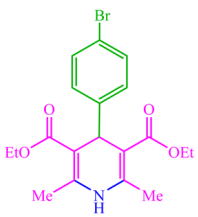 **4i**	10	77	10	78	162–165 (164–165) (28)
10	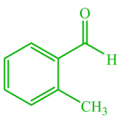	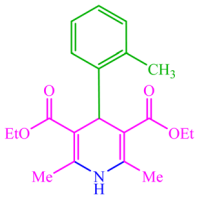 **4j**	20	90	—	—	178 (179) (28)

Table 2 (*Contd.*)

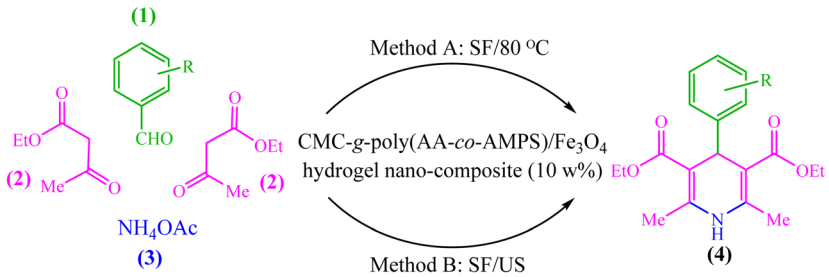

Entry	Aldehyde	Product	Method A[a] Time (min)	Method A[a] Yield[c] (%)	Method B[b] Time (min)	Method B[b] Yield[c] (%)	Mp (°C) (lit.)
11	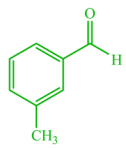	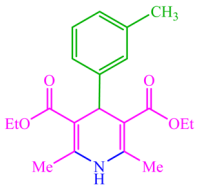 **4k**	15	85	—	—	126 (123–125) (55)
12	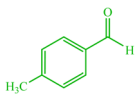	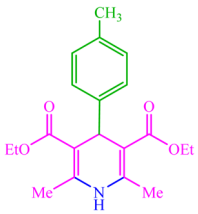 **4l**	15	80	10	82	135 (135) (28)
13	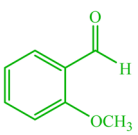	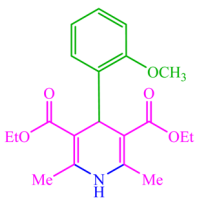 **4m**	30	80	10	95	156–158 (156) (28)
14	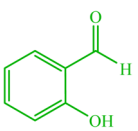	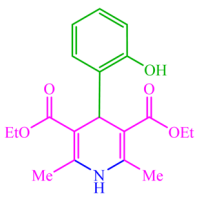 **4n**	30	83	10	96	118–120 (117–118) (57)
15	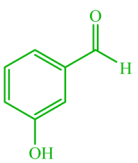	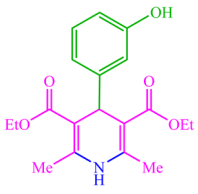 **4o**	15	98	10	98	186 (187–189) (58)

Table 2 (*Contd.*)

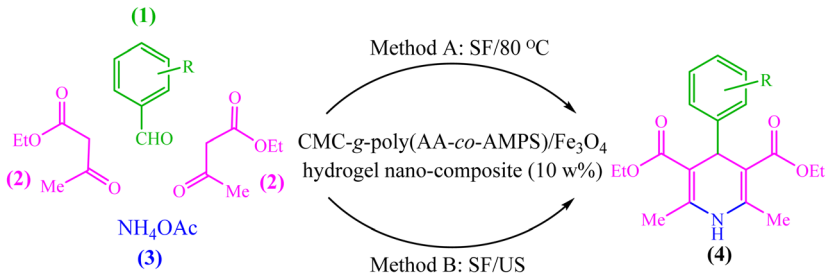

Entry	Aldehyde	Product	Method A[a] Time (min)	Method A[a] Yield[c] (%)	Method B[b] Time (min)	Method B[b] Yield[c] (%)	Mp (°C) (lit.)
16	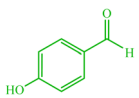	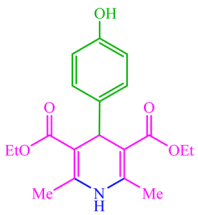 **4p**	10	98	10	98	223–226 (222) (28)
17	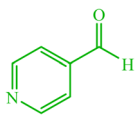	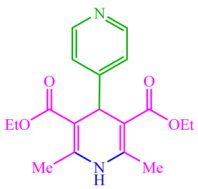 **4q**	15	92	10	93	177–180 (176–178) (59)
18	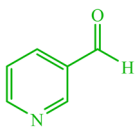	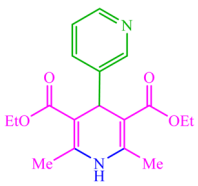 **4r**	15	90	10	90	190–192 (191–192) (60)
19	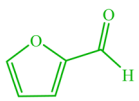	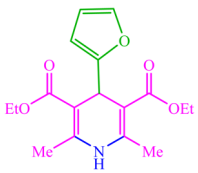 **4s**	10	90	10	92	160–163 (159–161) (59)
20	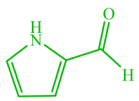	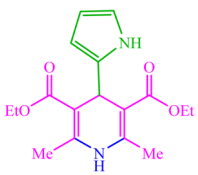 **4t**	10	87	10	90	210–212 (214–216) (60)

[a] Reaction conditions: benzaldehyde derivatives (1 mmol), ethyl acetoacetate (2 mmol), and ammonium acetate (1.5 mmol) at 80 °C. [b] Reaction conditions: benzaldehyde derivatives (1 mmol), ethyl acetoacetate (2 mmol), and ammonium acetate (1.5 mmol) at 40 °C under ultrasound-assisted conditions. [c] Isolated yields.

Table 3 A comparative performance of diverse nanocatalysts in the Hantzsch synthesis of 1,4-DHPs

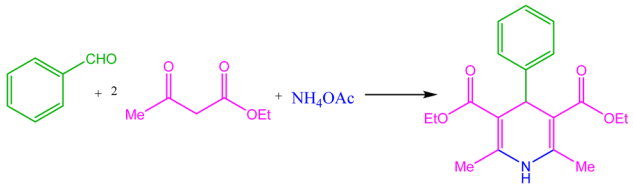

Entry	Catalyst	Reaction condition	Time (min)	Yield (%)	References
1	Chitosan nanoparticle (100 wt%)	Solvent free/80 °C	20	90	61
2	MWCNTs–$CONHCH_3$ (1 wt%)	EtOH/80 °C	240	85	62
3	Fe_3O_4/SiO_2–PDA nanocatalyst (50 wt%)	EtOH/US	10	89	58
4	γ-Fe_2O_3/Cu@cellulose nanobiocomposite (3 wt%)	Solvent free/RT	25	87	63
5	MCGC nanocatalyst (15 wt%)	EtOH/US	15	95	64
6	MCGC nanocatalyst (15 wt%)	EtOH/reflux	17	92	64
7	$CoFe_2O_4$@SiO_2–NH_2–Co^{II} nanoparticles (150 wt%)	H_2O, EtOH/reflux	150	85	65
8	BNPs@$SiO_2(CH_2)_3NHSO_3H$ nanocatalyst (60 wt%)	Solvent free/80 °C	30	97	66
9	COF–SO_3H nanoporous (20 wt%)	Solvent free/90 °C	10	93	55
10	Ch-rhomboclase nanocomposite (1.8 mol%)	Solvent free/80 °C	60	95	28
11	**CMC-*g*-poly(AA-*co*-AMPS)/Fe_3O_4 hydrogel nanocomposite (10 wt%)**	**Solvent free/80 °C**	**20**	**87**	**This work**
12	**CMC-*g*-poly(AA-*co*-AMPS)/Fe_3O_4 hydrogel nanocomposite (10 wt%)**	**Solvent free/US**	**10**	**90**	**This work**

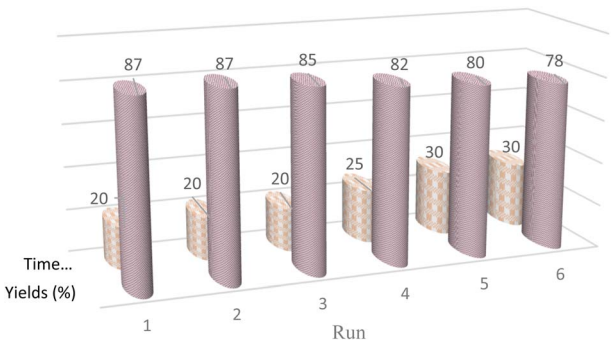

Fig. 6 Recyclability diagram of the CMC-*g*-poly(AA-*co*-AMPS)/Fe_3O_4 hydrogel nanocomposite in the Hantzsch synthesis.

$2CH_3$), 3.96 (m, 4H, $2CH_2$), 4.96 (s, 1H, CH), 7.51–7.95 (m, 4H, Ph), 8.97 (s, 1H, NH); ^{13}C NMR (75 MHz, DMSO-d_6) δ (ppm): 14.00, 18.19, 59.16, 101.06, 121.00, 121.90, 129.50, 134.21, 145.32, 147.39, 150.27, 166.47.

Diethyl 2,6-dimethyl-4-(4-nitrophenyl)-1,4-dihydropyridine-3,5-dicarboxylate (4c). Mp: 129–133 °C (127–132 °C[28]); ^{1}H NMR (300 MHz, DMSO-d_6) δ (ppm): 1.11 (t, 6H, $2CH_3$), 2.26 (s, 6H, $2CH_3$), 3.97 (m, 4H, $2CH_2$), 4.96 (s, 1H, CH), 7.38–8.11 (d of d, 4H, Ph), 8.97 (s, 1H, NH); ^{13}C NMR (75 MHz, DMSO-d_6) δ (ppm): 14.08, 18.19, 59.16, 100.79, 123.24, 123.55, 145.78, 146.26, 155.44, 166.47.

Diethyl 4-(4-cyanophenyl)-2,6-dimethyl-1,4-dihydropyridine-3,5-dicarboxylate (4d). Mp: 162–166 °C (166–167 °C[54]); ^{1}H NMR (300 MHz, DMSO-d_6) δ (ppm): 1.10 (t, 6H, $2CH_3$), 2.25 (s, 6H, $2CH_3$), 3.97 (m, 4H, $2CH_2$), 4.89 (s, 1H, CH), 7.30–7.68 (d of d, 4H, Ph), 8.93 (s, 1H, NH); ^{13}C NMR (75 MHz, DMSO-d_6) δ (ppm): 14.34, 18.49, 59.76, 101.87, 118.24, 125.55, 134.35, 145.78, 146.84, 155.41, 167.00.

Diethyl 4-(2-chlorophenyl)-2,6-dimethyl-1,4-dihydropyridine-3,5-dicarboxylate (4e). Mp: 214 °C (216–217 °C[55]); ^{1}H NMR (300 MHz, DMSO-d_6) δ (ppm): 1.10 (t, 6H, $2CH_3$), 2.26 (s, 6H, $2CH_3$), 3.96 (m, 4H, $2CH_2$), 4.83 (s, 1H, CH), 7.28–7.68 (m, 4H, Ph), 8.69 (s, 1H, NH); ^{13}C NMR (75 MHz, DMSO-d_6) δ (ppm): 14.05, 18.61, 59.18, 101.88, 124.68, 124.76, 128.43, 132.01, 144.57, 148.71, 155.44, 166.54.

Diethyl 4-(3-chlorophenyl)-2,6-dimethyl-1,4-dihydropyridine-3,5-dicarboxylate (4f). Mp: 137–140 °C (140 °C[28]); ^{1}H NMR (300 MHz, DMSO-d_6) δ (ppm): 1.09 (t, 6H, $2CH_3$), 2.25 (s, 6H, $2CH_3$), 3.97 (m, 4H, $2CH_2$), 4.82 (s, 1H, CH), 7.08–7.26 (m, 4H, Ph), 8.87 (s, 1H, NH); ^{13}C NMR (75 MHz, DMSO-d_6) δ (ppm): 14.05, 18.61, 59.16, 101.79, 124.80, 125.15, 132.13, 144.78, 148.67, 155.42, 166.47.

Diethyl 4-(4-chlorophenyl)-2,6-dimethyl-1,4-dihydropyridine-3,5-dicarboxylate (4g). Mp: 150–154 °C (150–152 °C[56]); ^{1}H NMR (300 MHz, DMSO-d_6) δ (ppm): 1.09 (t, 6H, $2CH_3$), 2.25 (s, 6H, $2CH_3$), 3.97 (m, 4H, $2CH_2$), 4.81 (s, 1H, CH), 7.10–7.23 (d of d, 4H, Ph), 8.85 (s, 1H, NH); ^{13}C NMR (75 MHz, DMSO-d_6) δ (ppm): 14.05, 18.61, 59.17, 101.78, 125.27, 132.34, 146.76, 155.28, 166.49.

Diethyl 4-(3-bromophenyl)-2,6-dimethyl-1,4-dihydropyridine-3,5-dicarboxylate (4h). Mp: 231–235 °C (230 °C[28]); ^{1}H NMR (300 MHz, DMSO-d_6) δ (ppm): 1.08 (t, 6H, $2CH_3$), 2.20 (s, 6H, $2CH_3$), 3.95 (m, 4H, $2CH_2$), 5.18 (s, 1H, CH), 6.97–7.41 (m, 4H, Ph), 8.80 (s, 1H, NH); ^{13}C NMR (75 MHz, DMSO-d_6) δ (ppm): 14.18, 19.16, 59.70, 102.32, 123.17, 126.73, 128.59, 129.38, 134.05, 145.08, 151.35, 167.18.

Diethyl 4-(4-bromophenyl)-2,6-dimethyl-1,4-dihydropyridine-3,5-dicarboxylate (4i). Mp: 162–165 °C (164–165 °C[28]); ^{1}H NMR (300 MHz, DMSO-d_6) δ (ppm): 1.11 (t, 6H, $2CH_3$), 2.24 (s, 6H, $2CH_3$), 3.97 (m, 4H, $2CH_2$), 4.82 (s, 1H, CH), 7.07–7.39 (d of d, 4H, Ph), 8.80 (s, 1H, NH); ^{13}C NMR (75 MHz,

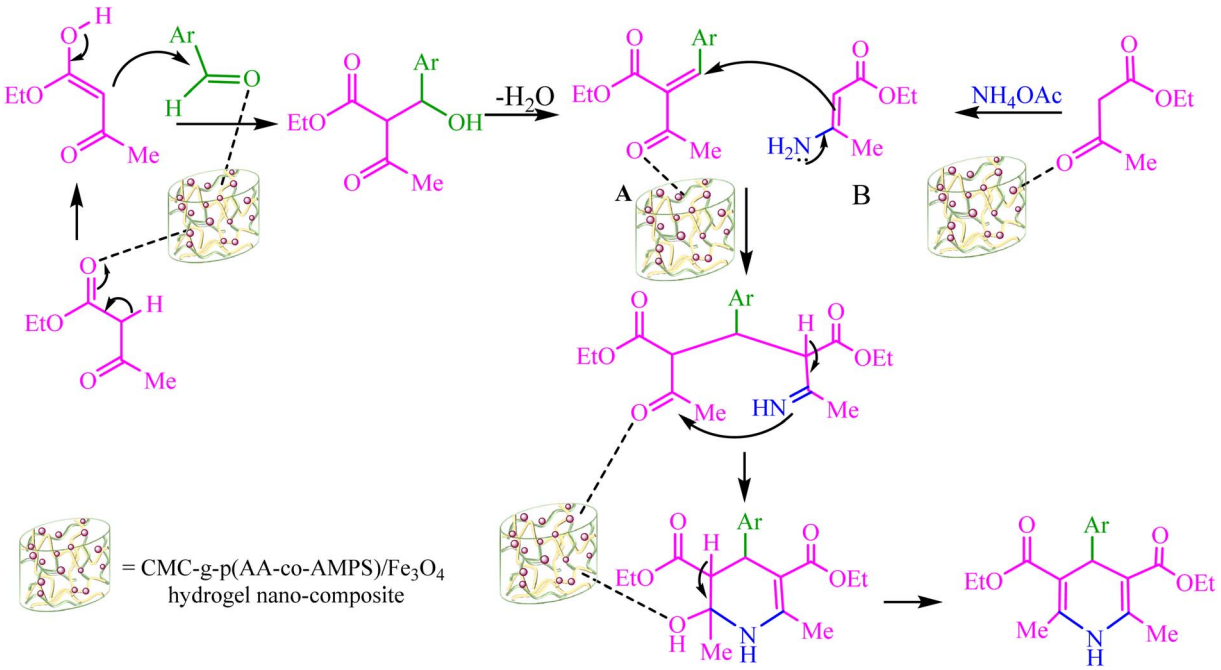

Scheme 3 Plausible mechanism for the Hantzsch synthesis of 1,4-DHP derivatives using the CMC-*g*-poly(AA-*co*-AMPS)/Fe_3O_4 hydrogel nanocomposite.

DMSO-d_6) δ (ppm): 14.18, 19.16, 59.70, 102.32, 121.04, 131.41, 131.64, 142.97, 150.71, 167.18.

Diethyl 2,6-dimethyl-4-(*o*-tolyl)-1,4-dihydropyridine-3,5-dicarboxylate (4j). Mp: 178 °C (179 °C[28]); ^{1}H NMR (300 MHz, DMSO-d_6) δ (ppm): 1.12 (t, 6H, $2CH_3$), 2.21 (s, 3H, CH_3), 2.24 (s, 6H, $2CH_3$), 3.97 (m, 4H, $2CH_2$), 4.91 (s, 1H, CH), 6.87–7.13 (m, 4H, Ph), 8.76 (s, 1H, NH); ^{13}C NMR (75 MHz, DMSO-d_6) δ (ppm): 14.17, 18.16, 18.31, 21.32, 58.96, 102.01, 122.63, 125.60, 135.78, 136.53, 145.24, 148.11, 166.97.

Diethyl 2,6-dimethyl-4-(*m*-tolyl)-1,4-dihydropyridine-3,5-dicarboxylate (4k). Mp: 126 °C (123–125 °C[55]); ^{1}H NMR (300 MHz, DMSO-d_6) δ (ppm): 1.12 (t, 6H, $2CH_3$), 2.21 (s, 3H, CH_3), 2.24 (s, 6H, $2CH_3$), 3.97 (m, 4H, $2CH_2$), 4.91 (s, 1H, CH), 6.90–7.09 (m, 4H, Ph), 8.74 (s, 1H, NH); ^{13}C NMR (75 MHz, DMSO-d_6) δ (ppm): 14.17, 18.16, 18.23, 21.20, 58.95, 101.85, 124.50, 126.53, 127.78, 128.04, 136.52, 145.24, 148.11, 166.97.

Diethyl 2,6-dimethyl-4-(*p*-tolyl)-1,4-dihydropyridine-3,5-dicarboxylate (4l). Mp: 135 °C (135 °C[28]); ^{1}H NMR (300 MHz, DMSO-d_6) δ (ppm): 1.12 (t, 6H, $2CH_3$), 2.22 (s, 3H, CH_3), 3.72 (s, 6H, $2CH_3$), 3.95 (m, 4H, $2CH_2$), 4.79 (s, 1H, CH), 6.96–7.02 (m, 4H, Ph), 8.71 (s, 1H, NH); ^{13}C NMR (75 MHz, DMSO-d_6) δ (ppm): 14.21, 18.23, 21.32, 59.16, 101.01, 124.51, 134.67, 145.03, 150.27, 166.97.

Diethyl 4-(2-methoxyphenyl)-2,6-dimethyl-1,4-dihydropyridine-3,5-dicarboxylate (4m). Mp: 156–158 °C (156 °C[28]); ^{1}H NMR (300 MHz, DMSO-d_6) δ (ppm): 1.12 (t, 6H, $2CH_3$), 2.21 (s, 6H, $2CH_3$), 3.81 (s, 3H, CH_3), 3.95 (m, 4H, CH_2), 4.78 (s, 1H, CH), 6.90–7.44 (m, 4H, Ph), 8.65 (s, 1H, NH); ^{13}C NMR (75 MHz, DMSO-d_6) δ (ppm): 14.02, 18.05, 18.31, 56.10, 58.87, 102.01, 112.21, 120.07, 125.14, 133.78, 135.37, 145.12, 148.04, 166.92.

Diethyl 4-(2-hydroxyphenyl)-2,6-dimethyl-1,4-dihydropyridine-3,5-dicarboxylate (4n). Mp: 118–120 °C (117–118 °C[57]); ^{1}H NMR (300 MHz, DMSO-d_6) δ (ppm): 1.12 (t, 6H, $2CH_3$), 2.22 (s, 3H, CH_3), 3.95 (m, 4H, $2CH_2$), 4.73 (s, 1H, CH), 6.53–7.15 (m, 4H, Ph), 8.65 (s, 1H, NH), 9.00 (s, 1H, OH); ^{13}C NMR (75 MHz, DMSO-d_6) δ (ppm): 14.02, 18.05, 36.90, 58.87, 101.85, 112.04, 120.01, 124.56, 133.48, 134.94, 145.11, 147.96, 166.47.

Diethyl 4-(3-hydroxyphenyl)-2,6-dimethyl-1,4-dihydropyridine-3,5-dicarboxylate (4o). Mp: 186 °C (187–189 °C[58]); ^{1}H NMR (300 MHz, DMSO-d_6) δ (ppm): 1.13 (t, 6H, $2CH_3$), 2.20 (s, 3H, CH_3), 3.95 (m, 4H, $2CH_2$), 4.70 (s, 1H, CH), 6.51–7.17 (m, 4H, Ph), 8.67 (s, 1H, NH), 9.01 (s, 1H, OH); ^{13}C NMR (75 MHz, DMSO-d_6) δ (ppm): 14.00, 18.07, 36.93, 58.83, 101.92, 112.04, 120.13, 124.55, 133.69, 134.89, 145.19, 148.06, 166.32.

Diethyl 4-(4-hydroxyphenyl)-2,6-dimethyl-1,4-dihydropyridine-3,5-dicarboxylate (4p). Mp: 222 °C (223–226 °C[28]); ^{1}H NMR (300 MHz, DMSO-d_6) δ (ppm): 1.12 (t, 6H, $2CH_3$), 2.22 (s, 6H, CH_3), 3.96 (m, 4H, $2CH_2$), 4.73 (s, 1H, CH), 6.54–6.92 (d of d, 4H, Ph), 8.65 (s, 1H, NH), 9.01 (s, 1H, OH); ^{13}C NMR (75 MHz, DMSO-d_6) δ (ppm): 14.01, 18.19, 59.15, 101.00, 124.11, 134.21, 145.03, 150.22, 166.47.

Diethyl 2,6-dimethyl-1,4-dihydro-[4,4′-bipyridine]-3,5-dicarboxylate (4q). Mp: 177–180 °C (176–178 °C[59]); ^{1}H NMR (300 MHz, DMSO-d_6) δ (ppm): 1.11 (t, 6H, $2CH_3$), 2.19 (s, 3H, CH_3), 3.95 (m, 4H, $2CH_2$), 4.97 (s, 1H, CH), 7.36–8.12 (d of d, 4H, Ph), 8.96 (s, 1H, NH); ^{13}C NMR (75 MHz, DMSO-d_6) δ (ppm): 14.10, 18.19, 59.01, 101.17, 123.31, 123.56, 145.77, 155.35, 166.51.

Diethyl 2′,6′-dimethyl-1′,4′-dihydro-[3,4′-bipyridine]-3′,5′-dicarboxylate (4r). Mp: 190–192 °C (191–192 °C[60]); ^{1}H NMR (300

MHz, DMSO-d_6) δ (ppm): 1.10 (t, 6H, $2CH_3$), 2.25 (s, 6H, $2CH_3$), 3.96 (m, 4H, $2CH_2$), 4.80 (s, 1H, CH), 7.35–8.22 (m, 4H, Ph), 8.71 (s, 1H, NH); ^{13}C NMR (75 MHz, DMSO-d_6) δ (ppm): 14.10, 18.19, 59.01, 101.06, 123.40, 134.82, 143.32, 146.07, 166.51.

Diethyl 4-(furan-2-yl)-2,6-dimethyl-1,4-dihydropyridine-3,5-dicarboxylate (4s). Mp: 160–163 °C (159–161 °C[59]); ^{1}H NMR (300 MHz, DMSO-d_6) δ (ppm): 1.12 (t, 6H, $2CH_3$), 2.26 (s, 3H, CH_3), 4.01 (m, 4H, $2CH_2$), 4.86 (s, 1H, CH), 6.12–7.36 (m, 3H, Ar), 8.90 (s, 1H, NH); ^{13}C NMR (75 MHz, DMSO-d_6) δ (ppm): 14.05, 18.19, 31.20, 59.17, 101.03, 105.16, 106.00, 140.10, 146.19, 148.17, 150.51, 166.04.

Diethyl 2,6-dimethyl-4-(1*H*-pyrrol-2-yl)-1,4-dihydropyridine-3,5-dicarboxylate (4t). Mp: 210–212 °C (214–216 °C[60]); ^{1}H NMR (300 MHz, DMSO-d_6) δ (ppm): 1.12 (t, 6H, $2CH_3$), 2.26 (s, 3H, CH_3), 4.01 (m, 4H, $2CH_2$), 4.85 (s, 1H, CH), 6.12–7.37 (m, 3H, Ar), 8.91 (s, 1H, NH), 10.53 (s, 1H, NH); ^{13}C NMR (75 MHz, DMSO-d_6) δ (ppm): 14.05, 18.19, 31.20, 59.17, 101.12, 105.14, 106.00, 140.21, 146.18, 148.17, 150.50, 166.04.

Conclusion

A biopolymer-based nanocatalyst, a CMC-*g*-poly(AA-*co*-AMPS)/Fe_3O_4 hydrogel nanocomposite, has been successfully synthesized by graft copolymerization of AA and AMPS onto CMC, followed by the cross-linking of $FeCl_3$/$FeCl_2$. The CMC-*g*-poly(AA-*co*-AMPS)/Fe_3O_4 hydrogel nanocomposite was analyzed by FT-IR spectroscopy, SEM, TEM, EDX analysis, TGA, and VSM, which emphasized the proposed structure, size, morphology, thermal stability, and magnetic properties. Biocompatibility, high reactivity, favorable recyclability, availability, and economy can be mentioned as the advantages of the green hydrogel nanocatalyst. The CMC-*g*-poly(AA-*co*-AMPS)/Fe_3O_4 hydrogel nanocomposite was applied as an effective catalyst for the synthesis of 1,4-dihydropyridine (1,4-DHP) under solvent-free conditions by both thermal and ultrasound methods. The noteworthy advantages of this method included green and mild reaction conditions, short reaction time, and high yields of products.

Conflicts of interest

There are no conflicts to declare.

References

1 M. S. Esmaeili, M. R. Khodabakhshi, A. Maleki and Z. Varzi, Green, Natural and Low Cost Xanthum Gum Supported Fe3O4 as a Robust Biopolymer Nanocatalyst for the One-Pot Synthesis of 2-Amino-3-Cyano-4H-Pyran Derivatives, *Polycyclic Aromat. Compd.*, 2021, **41**(9), 1953–1971.

2 J. Soni, A. Sethiya, N. Sahiba and S. Agarwal, Recent advancements in organic synthesis catalyzed by graphene oxide metal composites as heterogeneous nanocatalysts, *Appl. Organomet. Chem.*, 2021, **35**(4), e6162.

3 A. Rabiei, S. Abdolmohammadi and F. Shafaei, A green approach for an efficient preparation of 2,4-diamino-6-aryl-5-pyrimidinecarbonitriles using a TiO2–SiO2 nanocomposite catalyst under solvent-free conditions, *Z. Naturforsch., B: J. Chem. Sci.*, 2017, **72**(4), 241–247.

4 H. Liu, K. Wang, L. Zhang, X. Qian, Y. Li and Y. Li, Selectively recognizing organic semiconducting molecules on solid state molecular cages based on ZnOTCPP, *Dalton Trans.*, 2014, **43**(2), 432–438.

5 A. Pourjavadi and M. Kurdtabar, Effect of different bases and neutralization steps on porosity and properties of collagen-based hydrogels, *Polym. Int.*, 2010, **59**(1), 36–42.

6 M. Kurdtabar, G. Baghestani and G. R. Bardajee, Development of a novel thermo-responsive hydrogel-coated gold nanorods as a drug delivery system, *Gold Bull.*, 2019, **52**(1), 9–17.

7 M. Maity and U. Maitra, An easily prepared palladium-hydrogel nanocomposite catalyst for C–C coupling reactions, *J. Mater. Chem. A*, 2014, **2**(44), 18952–18958.

8 M. Kurdtabar and G. Rezanejade Bardajee, Stimuli-Responsive Hydrogel Based on Poly((2-Dimethylamino) Ethyl Methacrylate) Grafted onto Sodium Alginate as a Drug Delivery System, *Polym. Sci., Ser. B*, 2019, **61**(5), 642–652.

9 S. Hashmi, A. Mushtaq, R. M. Khan, R. Ahmed and Z. U. Ali, Synthesis and Application of Hydrogels for Oil-Water Separation, *Iran. J. Chem. Chem. Eng.*, 2022, 4075–4088.

10 P. Thoniyot, M. J. Tan, A. A. Karim, D. J. Young and X. J. Loh, Nanoparticle-Hydrogel Composites: Concept, Design, and Applications of These Promising, Multi-Functional Materials, *Adv. Sci.*, 2015, **2**(1–2), 1400010.

11 L. Bertolacci, P. Valentini and P. P. Pompa, A nanocomposite hydrogel with catalytic properties for trace-element detection in real-world samples, *Sci. Rep.*, 2020, **10**(1), 1–8.

12 M. Kurdtabar and G. Rezanejade Bardajee, Drug release and swelling behavior of magnetic iron oxide nanocomposite hydrogels based on poly(acrylic acid) grafted onto sodium alginate, *Polym. Bull.*, 2020, **77**(6), 3001–3015.

13 M. Kurdtabar, S. Saif Heris and M. Dezfulian, Characterization of a Multi-responsive Magnetic Graphene Oxide Nanocomposite Hydrogel and Its Application for DOX Delivery, *Chin. J. Polym. Sci.*, 2021, **39**(12), 1597–1608.

14 V. Ghobadifar, G. B. Marandi, M. Kurdtabar and G. R. Bardajee, Removal of Pb(II) and Cd(II) by MnFe2O4@SiO2@VTMS Nanocomposite Hydrogel from Aqueous Solutions, *J. Polym. Environ.*, 2023, DOI: **10.1007/s10924-022-02670-4**.

15 A. R. Modarresi-Alam, I. D. Inaloo and E. Kleinpeter, Synthesis of primary thiocarbamates by silica sulfuric acid as effective reagent under solid-state and solution conditions, *J. Mol. Struct.*, 2012, **1024**, 156–162.

16 M. Kurdtabar, H. Nezam, G. Rezanejade Bardajee, M. Dezfulian and H. Salimi, Biocompatible Magnetic Hydrogel Nanocomposite Based on Carboxymethylcellulose: Synthesis, Cell Culture Property and Drug Delivery, *Polym. Sci., Ser. B*, 2018, **60**(2), 231–242.

17 M. Kurdtabar, R. N. Koutenaee and G. R. Bardajee, Synthesis and characterization of a novel pH-responsive nanocomposite hydrogel based on chitosan for targeted drug release, *J. Polym. Res.*, 2018, **25**(5), 1–11.

18 S. Fakheri-Vayeghan, S. Abdolmohammadi and R. Kia-Kojoori, An expedient synthesis of 6-amino-5-[(4-hydroxy-2-oxo-2H-chromen-3-yl)(aryl)methyl]-1,3-dimethyl-2,4,6(1H,3H)-pyrimidinedione derivatives using Fe3O4@TiO2 nanocomposite as an efficient, magnetically separable, and reusable catalyst, *Z. Naturforsch., B: J. Chem. Sci.*, 2018, **73**(8), 545–551.

19 S. Abdolmohammadi and Z. Hossaini, Fe3O4 MNPs as a green catalyst for syntheses of functionalized [1,3]-oxazole and 1H-pyrrolo-[1,3]-oxazole derivatives and evaluation of their antioxidant activity, *Mol. Diversity*, 2019, **23**(4), 885–896.

20 A. R. Sardarian and I. D. Inaloo, 4-Dodecylbenzenesulfonic acid (DBSA) promoted solvent-free diversity-oriented synthesis of primary carbamates, S-thiocarbamates and ureas, *RSC Adv.*, 2015, **5**(93), 76626–76641.

21 A. R. Sardarian, I. Dindarloo Inaloo, A. R. Modarresi-Alam, E. Kleinpeter and U. Schilde, Metal-Free Regioselective Monocyanation of Hydroxy-, Alkoxy-, and Benzyloxyarenes by Potassium Thiocyanate and Silica Sulfuric Acid as a Cyanating Agent, *J. Org. Chem.*, 2019, **84**(4), 1748–1756.

22 A. S. Shahvelayati, I. Yavari and A. S. Delbari, Formation of thiazol-2(3H)-imines by reaction of α-amino acids, aroylisothiocyanates, and α-bromoketones in an ionic liquid, *Chin. Chem. Lett.*, 2014, **25**(1), 119–122.

23 F. Sheikholeslami-Farahani and A. S. Shahvelayati, Synthesis of unsaturated α-acyloxybenzothiazoleamides *via* the Passerini three-component reaction, *Comb. Chem. High Throughput Screening*, 2013, **16**(9), 726–730.

24 A. S. Shahvelayati, A. Ashouri and A. S. Delbari, Ionic Liquid as a Green Media for the One-Pot Synthesis of New α-Thiazolodepsipeptide Derivatives *via* a Four-Component Reaction, *Lett. Org. Chem.*, 2016, **13**(2), 100–106.

25 Y. Merroun, s. Chehab, A. El Hallaoui, R. Ghailane, S. Boukhris and A. Souizi, Tin pyrophosphate (SnP2O7): as a novel heterogeneous and highly efficient catalyst for the one pot-three component synthesis of tetrahydrobenzo[*b*]pyran and dihydropyran[*c*]chromene derivatives, *Iran. J. Chem. Chem. Eng.*, 2022, DOI: **10.30492/IJCCE.2022.562958.5619**.

26 V. Kadam, T. Choudhare, D. Wagare, d. Lingampalle and P. D. Netankar, Four components one-pot synthesis of new thiazoles and their biological screening for anti-tuberculosis activity, *Iran. J. Chem. Chem. Eng.*, 2023, DOI: **10.30492/IJCCE.2023.560875.5549**.

27 P. Ghamari kargar, G. Bagherzade and H. Eshghi, Introduction of a trinuclear manganese(iii) catalyst on the surface of magnetic cellulose as an eco-benign, efficient and reusable novel heterogeneous catalyst for the multi-component synthesis of new derivatives of xanthene, *RSC Adv.*, 2021, **11**(8), 4339–4355.

28 P. Kamalzare, B. Mirza and S. Soleimani-Amiri, Chitosan magnetic nanocomposite: a magnetically reusable nanocatalyst for green synthesis of Hantzsch 1,4-dihydropyridines under solvent-free conditions, *J. Nanostruct. Chem.*, 2021, **11**(2), 229–243.

29 D. Aute, A. Kshirsagar, B. Uphade and A. Gadhave, Ultrasound Assisted and Aluminized Polyborate Prompted Green and Efficient One Pot Protocol for the Synthesis of Hexahydroquinolines, *Polycyclic Aromat. Compd.*, 2022, **42**(4), 1375–1390.

30 L. Moradi and M. Zare, Ultrasound-promoted green synthesis of 1,4-dihydropyridines using fuctionalized MWCNTs as a highly efficient heterogeneous catalyst, *Green Chem. Lett. Rev.*, 2018, **11**(3), 197–208.

31 M. Feizpour Bonab, S. Soleimani-Amiri and B. Mirza, Fe3O4@C@PrS-SO3H: A Novel Efficient Magnetically Recoverable Heterogeneous Catalyst in the Ultrasound-Assisted Synthesis of Coumarin Derivatives, *Polycyclic Aromat. Compd.*, 2022, 1–16.

32 F. Zarei, S. Soleimani-Amiri and Z. Azizi, Heterogeneously Catalyzed Pechmann Condensation Employing the HFe(SO4)2.4H2O-Chitosan Nano-Composite: Ultrasound-Accelerated Green Synthesis of Coumarins, *Polycyclic Aromat. Compd.*, 2022, **42**(9), 6072–6089.

33 S. Abdolmohammadi, B. Mirza and E. Vessally, Immobilized TiO2 nanoparticles on carbon nanotubes: an efficient heterogeneous catalyst for the synthesis of chromeno[b]pyridine derivatives under ultrasonic irradiation, *RSC Adv.*, 2019, **9**(71), 41868–41876.

34 I. D. Inaloo and S. Majnooni, Eco-Efficient Ultrasonic-Responsive Synthesis of Primary O-Alkyl and O-Aryl Thiocarbamates Using Brønsted Acid Ionic Liquid [H-NMP][HSO4] in Aqueous Media at Room Temperature, *ChemistrySelect*, 2018, **3**(15), 4095–4100.

35 S. Soleimani-Amiri, F. Shafaei, A. Varasteh Moradi, F. Gholami-Orimi and Z. Rostami, A Novel Synthesis and Antioxidant Evaluation of Functionalized [1,3]-Oxazoles Using Fe3O4-Magnetic Nanoparticles, *J. Heterocycl. Chem.*, 2019, **56**(10), 2744–2752.

36 S. F. Taheri Hatkehlouei, B. Mirza and S. Soleimani-Amiri*, Solvent-Free One-Pot Synthesis of Diverse Dihydropyrimidinones/Tetrahydropyrimidinones Using Biginelli Reaction Catalyzed by Fe3O4@C@OSO3H, *Polycyclic Aromat. Compd.*, 2022, **42**(4), 1341–1357.

37 S. Soleimani-Amiri, M. Arabkhazaeli, Z. Hossaini, S. Afrashteh and A. A. Eslami, Synthesis of Chromene Derivatives *via* Three-Component Reaction of 4-hydroxycumarin Catalyzed by Magnetic Fe3O4 Nanoparticles in Water, *J. Heterocycl. Chem.*, 2018, **55**(1), 209–213.

38 H. Ghavidel, B. Mirza, S. Soleimani-Amiri and M. Manafi, New insight into experimental and theoretical mechanistic study on a green synthesis of functionalized 4H-chromenes using magnetic nanoparticle catalyst, *J. Chin. Chem. Soc.*, 2020, **67**(10), 1856–1876.

39 S. S. Amiri, M. Ghazvini, S. Khandan and S. Afrashteh, KF/Clinoptilolite@MWCNTs Nanocomposites Promoted a Novel Four-Component Reaction of Isocyanides for the Green Synthesis of Pyrimidoisoquinolines in Water, *Polycyclic Aromat. Compd.*, 2022, **42**(7), 4736–4751.

40 S. Soleimani-Amiri, Z. Hossaini and Z. Azizi, Synthesis and Investigation of Biological Activity of New

Oxazinoazepines: Application of Fe3O4/CuO/ZnO@MWCNT Magnetic Nanocomposite in Reduction of 4-Nitrophenol in Water, *Polycyclic Aromat. Compd.*, 2022, 1–22.

41 S. Soleimani-Amiri, Z. Hossaini and Z. Azizi, Synthesis and Investigation of Antioxidant and Antimicrobial Activity of New Pyrazinopyrroloazepine Derivatives Using Fe3O4/CuO/ZnO@ MWCNT MNCs as Organometallic Nanocatalyst by New MCRs, *Appl. Organomet. Chem.*, 2022, **36**(4), e6573.

42 N. Nasehi, B. Mirza and S. Soleimani-Amiri, Fe3O4@C@prNHSO3H: a novel magnetically recoverable heterogeneous catalyst in green synthesis of diverse triazoles, *J. Chin. Chem. Soc.*, 2021, **68**(11), 2071–2084.

43 E. Ezzatzadeh, S. Soleimani-Amiri, Z. Hossaini and K. Khandan Barani, Synthesis and evaluation of the antioxidant activity of new spiro-1,2,4-triazine derivatives applying Ag/Fe(3)O(4)/CdO@MWCNT MNCs as efficient organometallic nanocatalysts, *Front. Chem.*, 2022, **10**, 1001707.

44 M. Mahdavi, M. B. Ahmad, M. J. Haron, F. Namvar, B. Nadi, M. Z. Rahman and et al, ., Synthesis, surface modification and characterisation of biocompatible magnetic iron oxide nanoparticles for biomedical applications, *Molecules*, 2013, **18**(7), 7533–7548.

45 G. R. Bardajee and Z. Hooshyar, A novel biocompatible magnetic iron oxide nanoparticles/hydrogel based on poly (acrylic acid) grafted onto starch for controlled drug release, *J. Polym. Res.*, 2013, **20**(11), 298.

46 M. Helminger, B. Wu, T. Kollmann, D. Benke, D. Schwahn, V. Pipich and et al, ., Synthesis and Characterization of Gelatin-Based Magnetic Hydrogels, *Adv. Funct. Mater.*, 2014, **24**(21), 3187–3196.

47 M. T. Nakhjiri, G. B. Marandi and M. Kurdtabar, Adsorption of Methylene Blue, Brilliant Green and Rhodamine B from Aqueous Solution Using Collagen-*g*-p(AA-*co*-NVP)/Fe3O4@SiO2 Nanocomposite Hydrogel, *J. Polym. Environ.*, 2019, **27**, 581–599.

48 N. Jabeen, Z. H. Farooqi, A. Shah, A. Ali, M. Khurram, K. Mahmood and et al, ., Synthesis and characterization of cobalt nanoparticles containing anionic polymer hydrogel nanocomposite catalysts for fast reduction of nitrocompounds in water, *J. Porous Mater.*, 2021, **28**(5), 1563–1576.

49 M. A. Ashraf, W. Peng, Y. Zare and K. Y. Rhee, Effects of Size and Aggregation/Agglomeration of Nanoparticles on the Interfacial/Interphase Properties and Tensile Strength of Polymer Nanocomposites, *Nanoscale Res. Lett.*, 2018, **13**(1), 214.

50 Y. Chen, P. Pötschke, J. Pionteck, B. Voit and H. Qi, Fe3O4 Nanoparticles Grown on Cellulose/GO Hydrogels as Advanced Catalytic Materials for the Heterogeneous Fenton-like Reaction, *ACS Omega*, 2019, **4**(3), 5117–5125.

51 W.-Y. Chou, P.-H. Fang, W.-C. Chiang and H.-L. Cheng, Room temperature ferromagnetism in Fe3O4 nanoparticle-embedded polymer semiconductors, *J. Phys. Chem. Solids*, 2022, **167**, 110750.

52 S. Venkateswarlu and M. Yoon, Core-Shell Ferromagnetic Nanorod Based on Amine Polymer Composite (Fe3O4@DAPF) for Fast Removal of Pb(II) from Aqueous Solutions, *ACS Appl. Mater. Interfaces*, 2015, **7**(45), 25362–25372.

53 I. Karimzadeh, M. Aghazadeh, M. R. Ganjali, T. Doroudi and P. H. Kolivand, Preparation and characterization of iron oxide (Fe3O4) nanoparticles coated with polyvinylpyrrolidone/polyethylenimine through a facile one-pot deposition route, *J. Magn. Magn. Mater.*, 2017, **433**, 148–154.

54 P. Ghamari Kargar, M. Noorian, E. Chamani, G. Bagherzade and Z. Kiani, Synthesis, characterization and cytotoxicity evaluation of a novel magnetic nanocomposite with iron oxide deposited on cellulose nanofibers with nickel (Fe3O4@NFC@ONSM-Ni), *RSC Adv.*, 2021, **11**(28), 17413–17430.

55 R. Farsi, M. K. Mohammadi and S. J. Saghanezhad, Sulfonamide-functionalized covalent organic framework (COF-SO3H): an efficient heterogeneous acidic catalyst for the one-pot preparation of polyhydroquinoline and 1,4-dihydropyridine derivatives, *Res. Chem. Intermed.*, 2021, **47**(3), 1161–1179.

56 M. A. E. A. A. Ali El-Remaily, H. A. Hamad, A. M. M. Soliman and O. M. Elhady, Boosting the catalytic performance of manganese (III)-porphyrin complex MnTSPP for facile one-pot green synthesis of 1,4-dihydropyridine derivatives under mild conditions, *Appl. Organomet. Chem.*, 2021, **35**(7), e6238.

57 D. S. Rekunge, C. K. Khatri and G. U. Chaturbhuj, Sulfated polyborate: an efficient and reusable catalyst for one pot synthesis of Hantzsch 1,4-dihydropyridines derivatives using ammonium carbonate under solvent free conditions, *Tetrahedron Lett.*, 2017, **58**(12), 1240–1244.

58 R. Taheri-Ledari, J. Rahimi and A. Maleki, Synergistic catalytic effect between ultrasound waves and pyrimidine-2,4-diamine-functionalized magnetic nanoparticles: applied for synthesis of 1,4-dihydropyridine pharmaceutical derivatives, *Ultrason. Sonochem.*, 2019, **59**, 104737.

59 F. Tamaddon and S. Ghazi, Urease: a highly biocompatible catalyst for switchable Biginelli reaction and synthesis of 1,4-dihydropyridines from the *in situ* formed ammonia, *Catal. Commun.*, 2015, **72**, 63–67.

60 H. Niaz, H. Kashtoh, J. A. J. Khan, A. Khan, A.-t. Wahab, M. T. Alam and et al, ., Synthesis of diethyl 4-substituted-2,6-dimethyl-1,4-dihydropyridine-3,5-dicarboxylates as a new series of inhibitors against yeast α-glucosidase, *Eur. J. Med. Chem.*, 2015, **95**, 199–209.

61 J. Safari, F. Azizi and M. Sadeghi, Chitosan nanoparticles as a green and renewable catalyst in the synthesis of 1,4-dihydropyridine under solvent-free conditions, *New J. Chem.*, 2015, **39**(3), 1905–1909.

62 R. Mahinpour, L. Moradi, Z. Zahraei and N. Pahlevanzadeh, New synthetic method for the synthesis of 1,4-dihydropyridine using aminated multiwalled carbon nanotubes as high efficient catalyst and investigation of their antimicrobial properties, *J. Saudi Chem. Soc.*, 2018, **22**(7), 876–885.

63 A. Maleki, V. Eskandarpour, J. Rahimi and N. Hamidi, Cellulose matrix embedded copper decorated magnetic bionanocomposite as a green catalyst in the synthesis of dihydropyridines and polyhydroquinolines, *Carbohydr. Polym.*, 2019, **208**, 251–260.

64 K. Javanmiri and R. Karimian, Green synthesis of benzimidazoloquinazolines and 1,4-dihydropyridines using magnetic cyanoguanidine-modified chitosan as an efficient heterogeneous nanocatalyst under various conditions, *Monatsh. Chem.*, 2020, **151**(2), 199–212.

65 A. Allahresani, M. Mohammadpour Sangani and M. A. Nasseri, CoFe2O4@SiO2-NH2-CoII NPs catalyzed Hantzsch reaction as an efficient, reusable catalyst for the facile, green, one-pot synthesis of novel functionalized 1,4-dihydropyridine derivatives, *Appl. Organomet. Chem.*, 2020, **34**(9), e5759.

66 M. Khodamorady, S. Sohrabnezhad and K. Bahrami, Efficient one-pot synthetic methods for the preparation of 3,4-dihydropyrimidinones and 1,4-dihydropyridine derivatives using BNPs@SiO2(CH2)3NHSO3H as a ligand and metal free acidic heterogeneous nano-catalyst, *Polyhedron*, 2020, **178**, 114340.